

Design Optimization of Mechanical Valves in Dishwashers Based on the Minimization of Pressure Losses

Furkan Kılavuz^{1,2} – Binnur Gören Kırıl^{3,*}

¹ Dokuz Eylül University, The Graduate School of Natural and Applied Sciences, Turkey

² Arçelik A.Ş., Turkey

³ Dokuz Eylül University, Department of Mechanical Engineering, Turkey

Energy savings, albeit very small, are of great importance for devices whose use has become indispensable. In this study, an optimization based on sustainability and energy saving was aimed at designing the valve used in a white goods company's mass production of dishwashers. One significant factor that affects the overall efficiency of a dishwasher is pressure loss within the mechanical valve system. By optimizing the system, it is possible to minimize pressure loss and increase overall efficiency. To this end, 4th-order Bézier curves, which are used to model the blades of the impeller, were obtained using MATLAB R2023a software. Using Bézier curves, solid models of impellers with different blade profiles and numbers were created with SOLIDWORKS 2021 software. Fifty different models with six different blade numbers and five different materials were considered. In the numerical analyses, pressure losses were determined using ANSYS Fluent 2023R2 software. In addition to numerical analysis, blades were produced using the additive manufacturing method, and outlet pressures were measured experimentally. The experimental results were compared with the computational fluid dynamics analysis findings to evaluate the performance of different impeller designs. To determine the optimal design, the design of experiments and response optimizer approaches are applied, which enables the systematic evaluation of different design parameters. Furthermore, using numerical results, an artificial neural network model was created, and efficiency was predicted for the optimum parameters. Experimental and numerical results show that the optimum blade design enables the least pressure loss.

Keywords: dishwasher, energy-saving, impeller blade design optimization, statistical analysis, artificial neural network

Highlights

- The experimental setup for a bottom-up investigation of effect of impeller design in dishwasher was built.
- Design optimization of the mechanical valve impeller in dishwashers was made using Bezier curves.
- Both experimental setup and computational fluid dynamics analysis were performed to validate the design optimization.
- This paper studies the effect of parameters such as minimum pressure loss, maximum outlet pressure, and maximum efficiency for mechanical valve impellers used in dishwashers.
- The results of ANOVA, DOE, and regression analysis show that blade angles and the number of blades have significantly affect on the impeller design in the mechanical valve system.

0 INTRODUCTION

Dishwashers have become indispensable appliances in modern households, providing convenience and efficiency in the cleaning of dishes and utensils. The effectiveness of a dishwasher relies on various components, and the mechanical valve is a critical element responsible for directing and controlling the flow of water during the washing process. Pressure loss is the reduction in pressure experienced by water as it flows through the valve. Excessive pressure loss can result in decreased water flow rates, increased energy consumption, and compromised cleaning effectiveness. The design of the mechanical valve plays a crucial role in determining the pressure loss within the dishwasher system. By optimizing the design parameters, such as the number of blades and materials used in the gear mechanism, it is possible to minimize pressure loss and improve the overall

efficiency of the dishwasher. This study aims to investigate the impact of the mechanical valve design on pressure loss within dishwasher systems. The focus will be on modifying the number of blades and exploring different materials for the gear within the mechanical valve. By systematically varying these design parameters, the goal of the study is to determine the optimal configuration that minimizes pressure loss and maximizes water flow efficiency.

Although there is no study in the literature on the optimization of the blade design of the mechanical valve of dishwashers, some studies on the optimization of the blades and air foil have been done. Lu et al. [1] carried out the two multi-objective optimization designs of the rotor blade for an axial transonic compressor. Rengma et al. [2] developed a new method for creating wing shapes using a Bezier curve with six control points. Zhong et al. [3] proposed a unified formulation for the material optimization

and modelling of rotating in-plane functionally graded (IFG) thin-shell blades with variable thickness. Tang et al. [4] investigated a multivariate optimization design approach for the rotorcraft wing structure using computational fluid dynamics, neural networks, and evolutionary algorithms to improve the Mars rover's driving path. Using a supervised learning model approach, Luo et al. [5] investigated the aerodynamic design optimization of a transonic fan rotor by blade sweeping. Lu et al. [6] optimized the geometry of S-shaped blades used in Savonius turbines using genetic algorithms (GA) and numerical simulation of computational fluid dynamics (CFD). Fazil and Jayakumar [7] focused on leveraging the camber profile's control point to create an air foil profile using CATIA software. Fincham and Friswell [8] created an optimization technique for morphing aerofoils that took into consideration a known potential morphing system while still maintaining the aerodynamic optimization process. For wind turbine applications, Hansen [9] created and evaluated an air foil optimization technique that reduces performance loss from leading-edge contamination. To provide greater lift than the original air foil shape produces, Jeong and Kim [10] researched the optimization of the air foil shape.

Among the most relevant studies to the present study, Salimi et al. [11] emphasized the optimization of a regenerative pump with an S-shaped impeller using response surface methodology. They aimed to design and optimized a new S-shaped impeller. In their study, the design of experiments (DOE), the response surface methodology, and the box Behnken design (BBD) were utilized for optimization. Satjaritanun et al. [12] have researched that a pitched-blade, contra-rotating impeller, baffle-free tank with opposing inward flow is optimized using various designs of mixers derived from the Taguchi method. Mixing efficiency and torque were used to find the optimal design for the different specific gravities of solid particles employed in both experiments and CFD simulations. Mohammed et al. [13] have optimized the rotary blades for a wind-powered water pumping system. They investigated the blade parameters such as chord distribution length, angle of twist, tip speed ratio, power coefficient of the blade and attack angle.

The scope of this study is to find the optimal impeller design that minimizes outlet pressure drop while maximizing performance. This study employs a multifaceted approach to determine the optimal impeller design for mechanical valves in dishwashers. The combination of experimental testing, computational fluid dynamic (CFD) analysis,

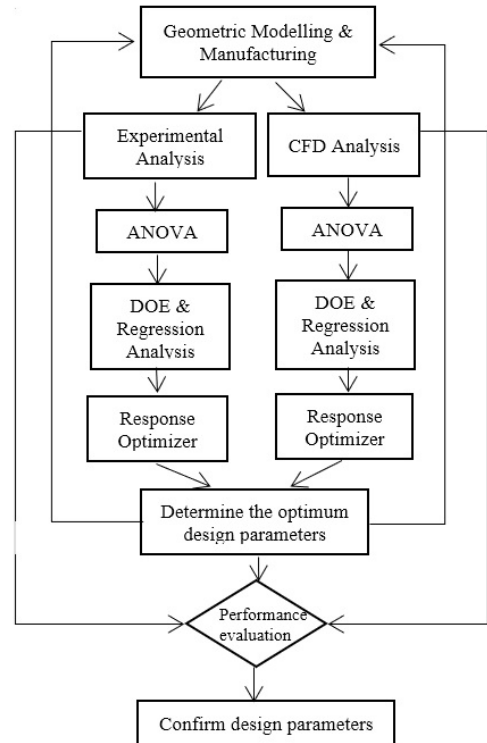


Fig. 1. Optimization procedure of the impeller

statistical analysis, and artificial neural network for a comprehensive assessment of the impeller performance and to identify the most effective design was used. By optimizing the number of blades and exploring different materials for the impeller, the study seeks to minimize the pressure loss and improve the water flow efficiency. The findings will contribute to the development of more efficient and environmentally friendly dishwasher designs, ultimately enhancing the overall performance and user experience of these essential household appliances. The findings of this study will provide valuable insights into the optimization of mechanical valve design for dishwashers. By minimizing pressure loss, manufacturers can enhance the performance and energy efficiency of dishwasher systems, contributing to sustainable water and energy consumption. Additionally, a better understanding of the fluid dynamics within the mechanical valve system can have wider implications for other applications involving flow control mechanisms.

1 MATERIALS AND METHODOLOGY

This research focuses on determining the optimal impeller design for the mechanical valve in

dishwashers using a comprehensive approach that integrates experimental testing, CFD analysis, statistical analysis, and artificial neural network analysis. In this study, the design of the impeller is based on Bézier curves, which are utilized to generate the blade profiles. 3D solid models of these designs are then created, printed with three-dimensional (3D) printers and tested in a special experimental setup. Fig. 1 shows a flowchart of the optimization studies carried out to determine the design parameters of the impeller to minimize pressure losses.

1.1 Creation of Blade Profiles Using Bézier Curve with MATLAB

The aim of this study is to design the surface of the blade profile of a centrifugal impeller, which provides a high performance to the impeller. Parametric examination studies have started to be carried out using Beziér curves used in the modelling of blade profiles. The Bézier’s technique is one of the most prominent in computer-aided geometric design. The fundamental aim is to determine curves that approach the given points rather than passing through them like a specific spline. Bézier curves have a useful convex formation that restricts the curve to never leave the bounding polygon of the control points. A Bézier curve of order n is defined by the Bernstein polynomials $B_{n,i}$:

$$P(u) = \sum_{i=0}^n B_{n,i}(u) P_i, \quad (1)$$

where the Bézier coefficients, are determined as follows:

$$B_{n,i}(u) = \frac{n!}{i!(n-i)!} u^i (1-u)^{n-i}, \quad (2)$$

and the point that corresponds to u on the Bézier curve is the “weighted” average of all control points, where the weights are the coefficients, $B_{n,i}$. The line segments, $P_0P_1, P_1P_2, \dots, P_{n-1}, P_n$ are called “control segments” [14] to [16]. A code was developed to obtain the control points using MATLAB R2023a software [17]. The blade profile was generated using 251 points obtained using MATLAB software; then a 3D solid model of the blade was created using SOLIDWORKS 2021 software [18].

The curvature of the blade profile to be optimized has been determined by a 4th degree of Bézier curve. The basic dimensions of the impeller are defined as the inner diameter is 5.53 mm and the outer diameter is 22 mm as given in Fig. 2. Fig. 3 shows the fundamental parameters, which are the control points

and installation angles to draw the blade profile. This figure also shows the wave form of the blade which has been determined by MATLAB software. As shown in the Fig. 3, points P_2 and P_3 are located at the midpoints between P_0 to P_5 and P_4 to P_5 , respectively. These points were used to define the equations of the Bézier curve.

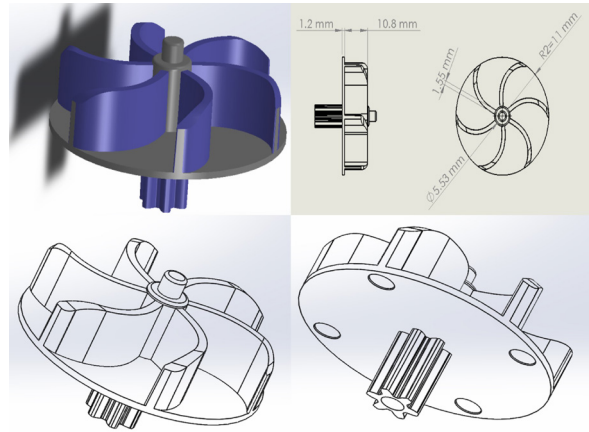


Fig. 2. Basic dimensions and solid model of the impeller

Angles β_1 and β_2 that are the fundamental parameters for modelling the blade shown in Fig. 3, are the impeller inlet and outlet installation angles. Blade profiles are selected in the range of $\beta_1 = 10^\circ$ to 30° and $\beta_2 = 10^\circ$ to 40° increasing 5° after the constraints in the modelling and studies in the literature are examined.

After the impeller blade profiles were created, three-dimensional solid models were generated by using SOLIDWORKS 2021 software. Fig. 4 shows the images of the solid models and graphs of the mass and mass moment of inertia values of the impellers for blade profiles of $\beta_1 = 10^\circ$ and $\beta_2 = 30^\circ$ exemplary. As seen from Fig. 4b, as the number of blades increases, the mass and mass moment of inertia of the blades increase slightly. The average power consumption is obtained by:

$$P = \frac{1}{T} \int_{\tau} M(t) \cdot \omega(t) dt, \quad (3)$$

where T is the time period, $M(t)$ is the torque [N·m] and $\omega(t)$ is the angular velocity of the impeller [rad/s] [19]. Under steady conditions, there is no torque imbalance meaning that the torque and angular acceleration are zero [20]. The required torque during the transient stage is calculated as follows:

$$M = I \cdot \frac{d\omega}{dt}, \quad (4)$$

where I is the mass moment of inertia with respect to shaft axis [$\text{kg}\cdot\text{m}^2$] and is the angular acceleration [rad/s^2]. The mechanical valve in this system is activated by pressurized water. Since the mass moment of inertia of the impeller is much smaller than the moment of pressurized water relative to the shaft axis, the required torque is exceeded in a short time, and the system starts to operate in a regular regime at a constant angular velocity. It has been seen from the literature that the rotational speed has more effect on the efficiency [19] and [20].

1.2 Materials

The material used in the mass production of the impeller examined in this study is polyoxymethylene (POM).

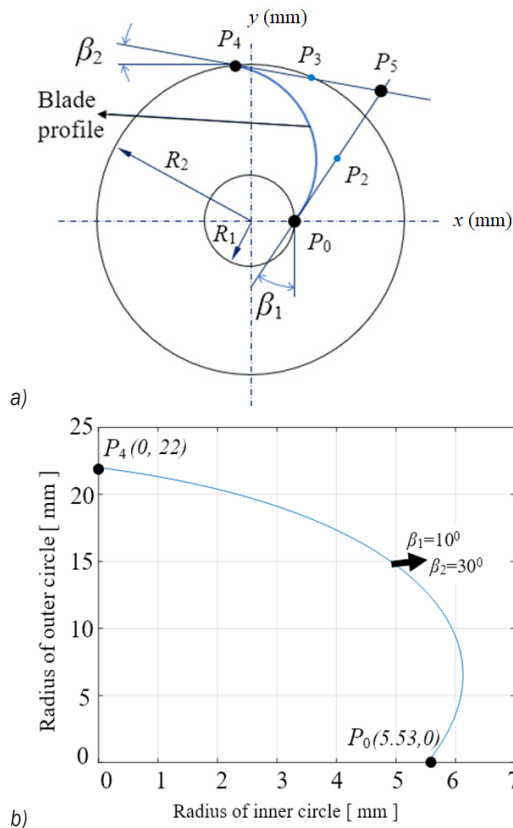


Fig. 3. a) Control points of the Bézier curve, and b) MATLAB image sample of the blade profile for $\beta_1 = 10^\circ$ & $\beta_2 = 30^\circ$

In this study, in addition to this material, impellers from polylactic acid (PLA), pure resin, resin reinforced with boron and graphene by the 0.1 % weight-ratio produced with a three-dimensional printer using fused deposition modelling (FDM) and stereolithography (SLA technologies were also produced. PLA, which

is the material of the impeller produced by FDM technology in this study, is a thermoplastic monomer obtained in the organic region such as polylactic acid, corn cab or sugar cane. Pure resin, which is the material of the impellers produced with SLA, is selected as a biocompatible resin that is safe in contact with food and not harmful to human health. Boron nitride and graphene particle additives were used to increase the strength of impellers produced with SLA and to reduce friction and, accordingly, pressure losses. Also noteworthy is the possibility of using graphene in the field of biomedicine, both in diagnostic and therapeutic areas. As a carrier of medicine, graphene oxide is characterized by high biocompatibility and excellent solubility. This allows for precise dosing of anti-inflammatory and anti-cancer agents as well as enzymes and mineral substances. Boron, which is among the most valuable natural resources in Turkey, provides a significant contribution to human health. Boron is needed in low amounts in the human body; it is a mineral taken from the outside by food and water [21] and [22].

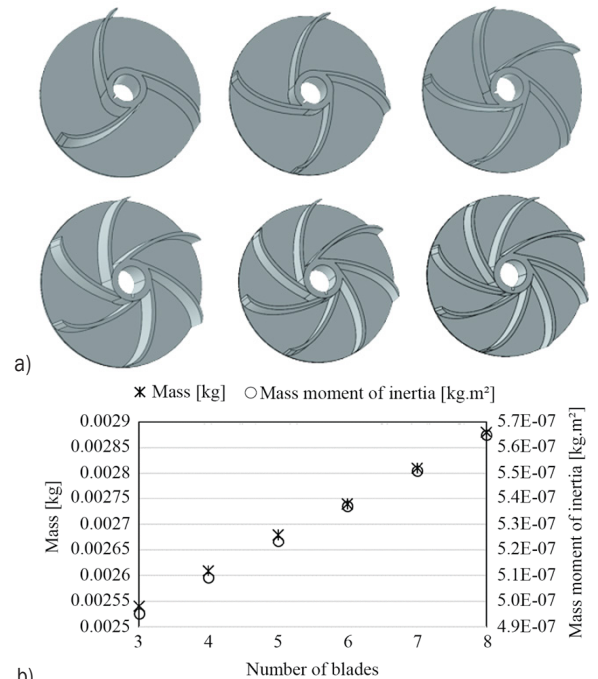


Fig. 4. a) Solid models; and b) mass and mass moment of inertia values of the impellers for blade profiles of $\beta_1 = 10^\circ$ and $\beta_2 = 30^\circ$.

Table 1 presents the material properties and dimensions of the reinforced particles used in this study. The resin used in the SLA process is biocompatible. The resin with methacrylate-based

Table 1. Material properties of impellers

Material	Modulus of Elasticity [MPa]	Tensile strength [MPa]	Elongation [%]
Resin with methacrylate-based compounds methacrylate [23]	1933.322	52.402	5.378
POM [24]	3150	48.5	25
PLA [25]	3500	50	7

Particle	Size [nm]	Purity [%]
Graphene nanoplatelet [26]	6	99.9
Boron nitride [27]	450	99.55

compounds methacrylate is also used for the fixation of monomer resin, dental materials, and prosthetic devices in orthopaedic surgery [23].

Fig. 5 shows examples of mechanical valve impellers produced in real dimensions with SLA and FDM technologies, using different materials for pressure measurements over the dishwasher. As an example, the assembly of the impeller produced by the SLA method using resin reinforced by graphene and original impeller made of POM used in the mass production to the mechanical valve is shown in Fig. 6.

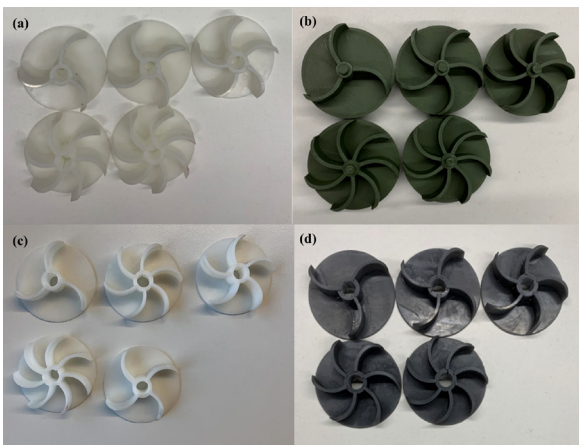


Fig. 5. Impellers produced using: a) pure resin, b) PLA, c) resin reinforced by boron, and d) resin reinforced by graphene by the additive manufacturing technology

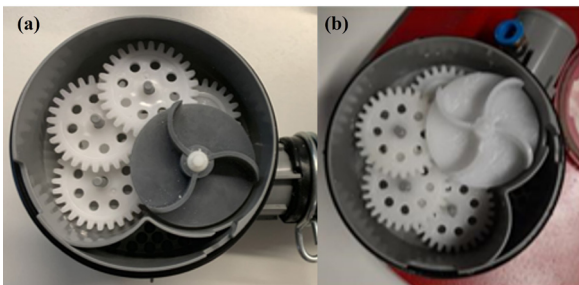


Fig. 6. Installation of the impeller to the valve system; a) impeller made of resin reinforced by graphene, and b) impeller made of POM

To determine whether the roughness of the surfaces would affect the flow, images of the blade surfaces of the propellers were taken with an optical microscope. Fig. 7 shows the images of the blades made of materials used in this study. The most roughness is seen on the blade surface made of PLA using FDM, as expected. However, considering the scale, it is calculated that the maximum value of the distance between the bottom surface and the top point can be approximately 70 μm . Images were obtained at many different magnification values, and only images magnified five times are presented in this study. Zhou et al. stated that the effect of surface roughness on pressure drop was negligible at low speeds, while pressure drop decreases with surface roughness at higher speeds in their study [28]. As a result, it was concluded that the geometric parameters of the blade are more dominant than the roughness on the pressure drop.

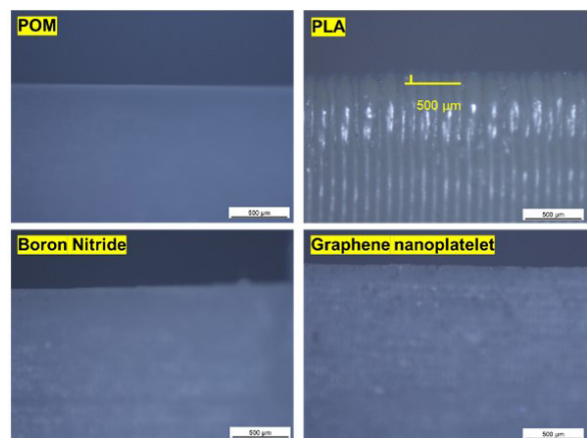


Fig. 7. Optical microscopy images of the blade surfaces

2 EXPERIMENTAL WORK

In this study, a specialized experimental setup was designed to measure the outlet pressure from the mechanical valve. Water from the dishwasher reservoir was passed through the mechanical valve, utilizing the

blade and gear systems. Pressure measurements were taken at the valve's outlet using a calibrated nozzle.

Experimental studies were conducted under two different fixed input pressures (300 mbar and 350 mbar). Previous studies have explored dishwasher water distribution systems and various valve designs. Electric motor-driven valves are commonly used due to their precise control capabilities, but their high cost and complexity have prompted research into alternative mechanical valves.

Fig. 8 exhibits the experimental methods in this study. The experimental setup consists of a water tank (#1), circulation pump (#2), pressure adjustment valve (#3), flow meter (EMFM HFD3000 electromagnetic flow meter, #4), dishwasher body (#5), sump group mounted on this body and mechanical valve within the chamber group (#6), pressure transmitter to measure the inlet pressure of the water before the mechanical valve (#7), pressure transmitter to measure the pressure in the outlet impeller (#8), and digital pressure gage (WIKA, #9). WIKA cph 6200 model having 0.2 % accuracy with calibration certificate was used in the measurements of the outlet pressure.

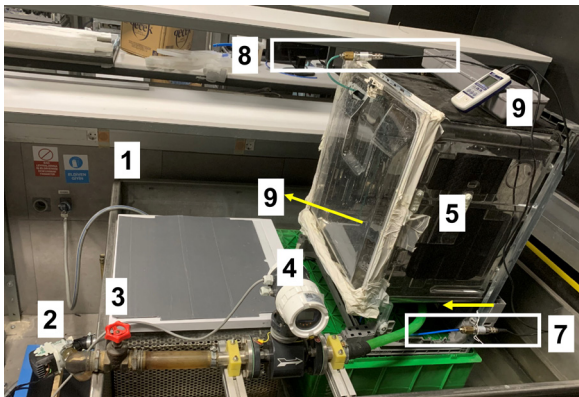


Fig. 8. Experimental setup

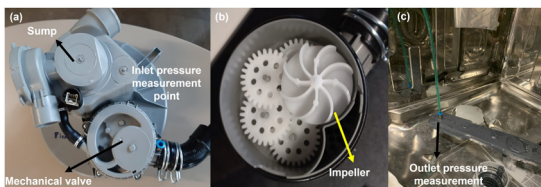


Fig. 9. a) Sump group with mechanical valve and inlet pressure measurement point, b) mechanical valve inside with impeller, and c) outlet pressure measurement point at lower spray arm

In the test system, water comes from the tap to the tank via the circulation pump. The circulation pump sucks the water from the tank and sends the water to the valve in the experimental setup. The pressure

adjustment valve provides adjusting the water pressure at the inlet pressure. In addition, before water is not entering the system, the flow meter is measured using an electromagnetic flow meter (EMFM). An inlet pressure transmitter in the system provides to adjust inlet water pressure at the mechanical valve entering. The outlet pressure transmitter provides a reading of the outlet water pressure at the lower spray arm; 300 mbar and 350 mbar water inlet pressure have been applied for experiment studies. The sump group with a mechanical valve was assembled into the dishwasher body. The sump group, mechanical valve system, and inlet/outlet pressure measurement points are shown in Fig. 9.

2.1 Numerical Examinations (CFD Analyses, Optimization and Artificial Neural Networks)

In this study, the modeling of the impeller was carried out using SOLIDWORKS software. To obtain the outlet pressure, the outlet velocity and forces acting on the blade were obtained by performing the CFD analyses by ANSYS Fluent 2023R2 [29].

The first stage of the numerical studies consists of determining the parameters of the blade by design of experiments (DOE) in Minitab® 21.1 statistical software [30]. The parameters were determined with the DOE method used to structure and organize an experiment using scientific methods and statistical techniques. DOE is a powerful research method used in scientific research, product and process improvement, quality control, and more. It contributes to the advancement of science and the solution of problems by helping to obtain efficient and accurate results. The purpose is to analyze the data obtained by carrying out experiments in a systematic and planned manner and to obtain accurate, reliable and statistically supported outcomes from the results. The main purpose of the DOE is to design and conduct experiments in a thoughtful and planned way rather than being random or unplanned. Therefore, it aids in using time and resources efficiently by collecting the less amount of data to obtain accurate results. DOE has been prepared for β_1 , β_2 and blade number inputs, which affect the impeller design. The analysis range was determined for each parameter. The maximum and minimum states for all inputs are defined in the analysis. It is introduced to the system that these inputs yield the maximum pressure output, because the higher the output pressure, the lower the pressure loss will be. As the pressure loss decreases, the washing performance of the system will increase.

Table 2. Case setup variables in design of experiments (DOE) which has the design angles (β_1, β_2) and number of blades

β_1 , inlet installation angle [deg]	β_2 , outlet installation angle [deg]	Number of blades
10	30	4
30	30	4
10	40	4
30	40	4
10	30	8
30	30	8
10	40	8
30	40	8

As a result, all of the design cases in the above-mentioned DOE are created, and the DOE parameter details are mentioned in Table 2. Three-dimensional solid models of the impellers were created with SOLIDWORKS according to the parameters given in Table 2. Using these models, CFD analyses were performed with the help of ANSYS Fluent 2023R2 software. From these analyses, outlet pressure, outlet velocity, and force values acting on the blades were determined. The optimization phase was carried out using the output pressure findings, which is the most important performance indicator. Response optimizer approaches were exploited to determine the effects of the design parameters on valve performance.

In this study, an artificial neural network (ANN) is also used to predict the outlet pressure for various blade models and the optimum blade profile obtained by ANOVA analysis. For this purpose, the MATLAB neural network fitting application [31] and [32] was used to compare the experimental and numerical results. Several ANN analyses using different numbers of hidden layers, and dual and triple combinations of transfer functions such as logarithmic sigmoid, tangent sigmoid, linear algorithms, ratio of training, validation, and testing were carried out to obtain the best ANN architecture. The ANN parameters used in this study correspond to the values at which the minimum error is obtained. The following transfer functions and other parameters defined are the parameters obtained as a result of various analyses. In the network architecture, the Levenberg-Marquardt back-propagation algorithm was used because learning of the network with this algorithm is faster than the gradient descent algorithm for data fitting [33]. The multilayer artificial neural network receives three parameters, which are impeller inlet and outlet installation angles at five ranks as inputs and then yields the estimation of the outlet estimation through the activation function. The Levenberg-Marquardt back-propagation algorithm is

then operated with the performance function, which is a function of the ANN-based weight and bias variables were adjusted according to the Levenberg-Marquardt method, and the back-propagation algorithm is used to calculate the Jacobian matrix of the performance function with respect to the weight and bias variables. With updated weights and biases, the ANN further estimates the output values such as outlet pressure and efficiency of the impeller. Using the outlet pressure data obtained via the CFD analyses, outlet pressure values for different impeller parameters were estimated with the help of the ANN method. The neural network consisting of an input layer, two hidden layers, and an output layer was used. In the training of neural networks, input and output values are frequently scaled to a range 0 to 1, which is called the normalisation process [31] and [32], which process is done separately for all network input and output values. First, each value was subtracted from the smallest number in Table 5 and then divided by the difference between the largest and smallest number in the table. The hidden and output layers of the ANN were modelled using logarithmic sigmoid, tangent sigmoid and positive linear transfer functions, respectively. The ideal number of neurons in the hidden layers was obtained as 9. The learning process of the network model was completed in the 220-epoch based on the mean square error method. The program automatically generates the initial weights and biases of the network. A total of 40 data points were selected to evaluate the performance of the trained network model.

3 RESULTS AND DISCUSSION

3.1 Experimental Results

Experimental studies in this paper consist of two parts. In the first step, outlet pressure values were measured for the original blade design used in mass production using the different materials and six different number of blades. In the second step, outlet pressure was measured using an impeller having the optimal blade profile obtained with flow analyses in ANSYS Fluent and response optimizer analyses in ANOVA.

In the first stage, with the experimental setup shown in Fig. 8, the outlet pressure values were measured at 300 mbar and 350 mbar water inlet pressure to see only the effect of the number of blades and the raw material of the impeller. The goal was to determine how the impellers produced with different number of blades and different raw materials affect the outlet pressure taken from the lower spray arm of the

system and to keep the pressure loss to a minimum. In the experimental examinations, the point where the inlet pressure was adjusted at 300 mbar and 350 mbar is shown in Fig. 8a. The outlet pressure of the water entering the mechanical valve system after the mechanical valve is measured from the nozzle shown in Fig. 8c on the lower impeller. Experiments were repeated 20 times at both 300 mbar and 350 mbar inlet pressures to measure the output pressure and flow rate for each impeller type. In the numerical investigations, the pressure value on the blade was determined and a correlation was attempted between the numerical and experimental findings. Considering the pressure drop of the water during the operation of the dishwasher, experimental studies were carried out for two different constant inlet pressures of 300 mbar and 350 mbar. The nominal inlet pressure in the washing state of the dishwasher is 350 mbar. The first element of the mechanical valve to encounter water is the impeller and the current design of this part has eight blades. In the first stage of the experimental studies, the difference between inlet and outlet pressures was determined in the case of the existing impeller made of POM material having eight and four blades. Different designs for this material could not be examined comprehensively due to mold costs and the effect of the number of vanes was investigated with alternative materials used in the additive manufacturing method. In the later stages of the study, it was aimed to reduce pressure losses by examining the design parameters of the impeller geometry. Fig. 10 shows the variation of the outlet pressure with respect to the inlet pressure for the current impeller made of POM having eight blades

used in mass production. Pressure losses differences in the system can be easily seen from the figure.

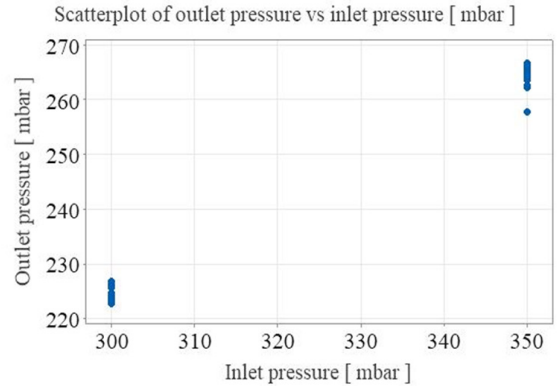


Fig. 10. Comparison of outlet pressure with respect to the inlet pressure for current impeller with eight blades

When 300 mbar inlet pressure is applied, the average outlet pressure is 224.44 mbar, while the average outlet pressure is 263.71 mbar when 350 mbar inlet pressure is applied. Under 300 mbar inlet pressure conditions, an average of 25.19 % pressure loss can occur, while under 350 mbar inlet pressure conditions, 24.65 % pressure loss can occur.

Within the scope of this study, impellers with the current blade design were also produced by the additive manufacturing method using different materials. The materials used in the additive manufacturing process are PLA in FDM, pure resin, and resin reinforced by both boron nitride and graphene nanoplatelet having nanosized in SLA. The

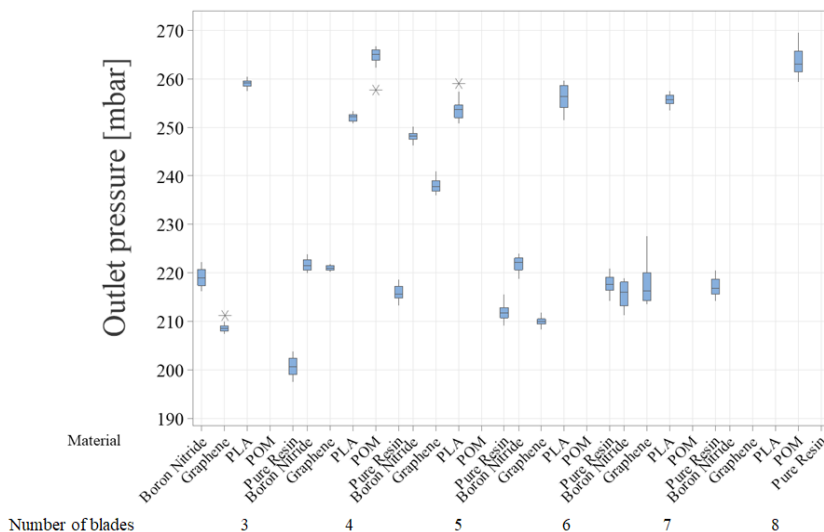


Fig. 11. Comparison of outlet pressure at 350 mbar inlet pressure according to related materials and number of blades respect to the inlet pressure for current impeller with eight blades

motivation for the use of boron and graphene was to reduce the friction coefficient of the blade surface and consequently reduce the inlet-outlet pressure differences. In addition to using different materials, 3-, 4-, 5-, 6-, 7- and 8-bladed impellers with existing blade profiles were produced to investigate the effect of the blade number at this stage of the study. Fig. 11 shows a comparison of the outlet pressure at 350 mbar inlet pressure according to related materials and the number of blades with respect to the inlet pressure for the current impeller with eight blades.

The regression equations for all impeller types obtained by ANOVA at 350 mbar pressure depending on the number of blades are shown in Fig. 12. As can be seen, while the outlet pressure has the lowest value for all blade numbers when the impeller produced using graphene nanoplatelet doped resin is used, the least pressure loss occurred when impellers made of PLA material were used.

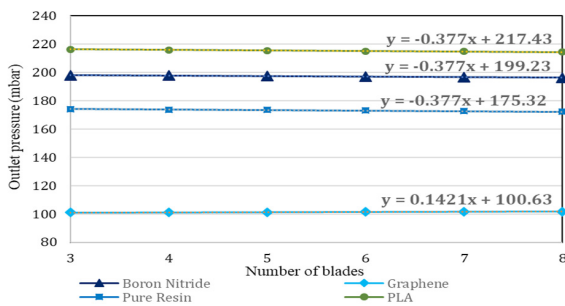


Fig. 12. Regression equations expressing the outlet pressure depending on the number of blades

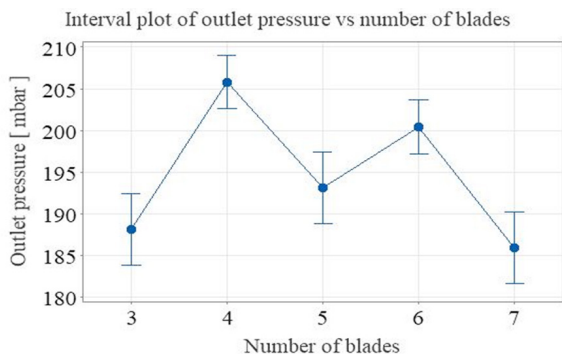
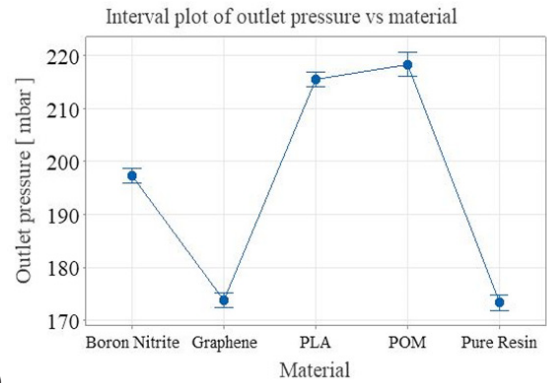


Fig. 13. Number of blades-outlet pressure box plot graph for 350 mbar inlet pressure for PLA material

Figs. 12 to 14 summarize the measurement results for outlet pressure performed at an inlet pressure of 350 mbar.



a)

Model Summary

S	R-sq	R-sq(adj)	R-sq(pred)
7.32905	86.77 %	86.65 %	86.47 %

b)

Fig. 14. a) Material-Outlet pressure graph; and b) regression analysis R-sq(adj) values at 350 mbar inlet pressure

3.2 Numerical Results

At this stage of the study, extensive analyses were carried out to determine the effect of the profile and number of blades on the pressure losses, outlet velocity, and force acting on the blade. As mentioned in Section 1, first, using Bezier curves, impellers with different blade profiles were modelled in three dimensions using SOLIDWORKS software. Flow analysis was performed with ANSYS Fluent CFD using the solid models obtained. Before solid models were created, design parameters were determined using the DOE tool in Minitab and models were created for these parameters. Then, using the data obtained from the flow analyses, the optimum design was determined using the ANOVA Response Optimizer tool. Flow analysis of this optimum design was also performed. Finally, this impeller, having the optimum design, was manufactured from PLA material with FDM technology, and the outlet pressure was measured experimentally.

3.2.1 Creation of Flow Volume and Definition of Boundary Conditions

Fig. 15 shows the boundary conditions of the impeller used in the CFD analyses. For the analyses, a cylindrical flow volume was first created with a porous jump to simulate pressure loss in the system and then an angular speed of 550 rpm was defined for the impeller around its shaft axis. Inlet flow rate and outlet pressure were defined as 0.675 kg/s and 0 Pa, respectively. Unlike experimental studies, since it is not possible to simulate the system exactly, the

Table 3. Mesh parameters

	Surface mesh size		Volume mesh size		Mesh metric					
	Min [mm]	Max [mm]	Max [mm]	Min [mm]	Max aspect ratio	Average aspect ratio	Minimum orthogonal quality	Average orthogonal quality	Max skewness	Average skewness
Mesh#1	0.2	12.8	6.4	0.8	76.3	6.36	0.15	0.88	0.85	0.12
Mesh#2	0.1	6.4	3.2	0.4	85.53	4.22	0.15	0.92	0.85	0.08

pressure value on the blade of the impeller was determined in numerical analysis, and explanations were attempted using these values. Exemplary, the minimum orthogonal mesh quality of the related six-bladed impeller is 0.153, the maximum aspect ratio is 58, and the maximum skewness is 0.64; the finite volume model of this impeller has 897,484 nodes and 282,049 computational cell numbers. In the flow analysis, an attempt was made to create a finite volume model with the same size volume for all the impeller models.

As the control parameter, the total pressure at the outlet condition and the total pressure at the inlet condition of the flow volume where the blades are located were taken and attempts were made to bring them to the maximum value. The function of “ $f(x) = Total\ pressure_{outlet} - Total\ pressure_{inlet}$ ” was tried to be maximized.

To reduce the computational cost of the optimization problem, the analysis was carried out in a steady state, independent of time. The frame motion [mrf (multiple reference frame)] option suitable for this setting is given to the flow volume in the selected impellers. Inlet condition is mass flow inlet and normal to the boundary. The outlet condition is

the pressure outlet with 0 Pa direction is normal to the boundary.

The viscous model and material have been selected as $k\omega$ -shear stress transport (SST) turbulence model and the water-liquid whose density is 998.2 kg/m³, respectively. Rhie-Chow interpolation method has been used as the flux type method in CFD calculations. Standard initialization from inlet has been used. The run calculation method is pseudo-transient, and the number of calculations is 400. The temperature of the fluid is 20 °C.

In this study, mesh independence analysis was performed. Table 3 shows the surface mesh size, volume mesh size, maximum and average aspect ratio values, minimum and average orthogonal quality values, and maximum and average skewness values for two different mesh sizes taken into consideration.

Table 4. Comparison of pressure results versus the mesh type

	Pressure inlet [mbar]	Pressure outlet [mbar]	Pressure loss, ΔP [mbar]
Mesh1	131.97	0.0342	131.94
Mesh2	129.39	0.0257	129.39

Table 4 presents the pressure difference between the inlet and outlet for the two mesh sizes. As seen,

Table 5. Results of flow analyses depending on the number of blades, β_1 and β_2 variables

	Number of blades	$\beta_1 = 10^\circ$	$\beta_1 = 10^\circ$	$\beta_1 = 20^\circ$	$\beta_1 = 20^\circ$	$\beta_1 = 25^\circ$	$\beta_1 = 25^\circ$	$\beta_1 = 30^\circ$	$\beta_1 = 30^\circ$	
		$\beta_2 = 30^\circ$	$\beta_2 = 40^\circ$							
Total pressure losses ΔP [mbar]	3	132.58	132.55	132.55	132.54	132.64	132.55	132.64	132.56	
	4	132.62	132.35	132.43	132.37	132.56	132.43	132.58	132.47	
	5	132.50	132.25	132.35	132.33	132.50	132.30	132.54	132.34	
	6	132.28	132.10	132.27	132.19	132.38	132.12	132.44	132.19	
	7	132.18	132.01	132.29	132.08	132.39	132.11	132.47	132.16	
	8	132.11	131.94	132.28	132.04	132.43	132.09	132.67	132.21	
	Efficiency of related impellers [%]	3	41.19	48.43	43.49	46.27	39.66	46.90	38.73	46.01
		4	54.65	63.44	58.30	60.59	51.04	60.15	50.61	57.85
5		63.90	72.70	66.30	67.09	58.23	69.73	55.46	67.47	
6		71.37	80.14	71.73	75.47	66.18	78.24	62.38	75.84	
7		76.96	83.60	72.03	80.65	66.53	80.91	62.42	77.83	
8		80.40	86.57	72.91	82.95	65.39	81.24	55.43	76.31	

there is a 1.95 % difference between two analyses. It is concluded from the analyses that mesh independence has been provided.

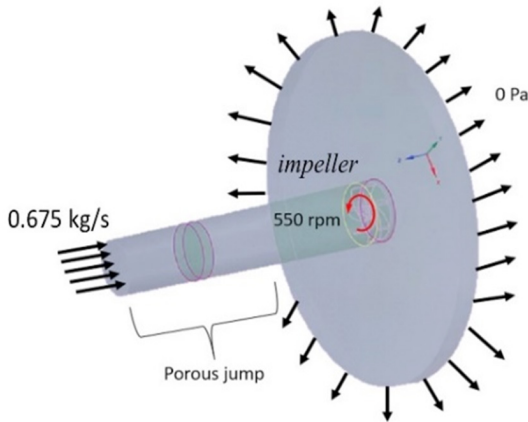


Fig. 15. Boundary conditions

Table 5 shows the results obtained from the CFD analysis for 48 different cases. These results will be evaluated with the statistical analyses performed by Minitab, and the optimum design will be selected. The analysis shows that the impeller with the optimum design should have 4.85 blades, which means approximately five blades according to the experimental results, in order to obtain the maximum outlet pressure shown in Figure 16. Among the raw materials that have been experimentally studied, PLA raw material can have the maximum effect on the outlet pressure.

Percent impeller efficiency is calculated by using Eq. (5) as follows:

$$\% \text{ efficiency} = \frac{P_{\text{discharge}} - P_{\text{suction}}}{P_{\text{discharge}}} \times 100. \quad (5)$$

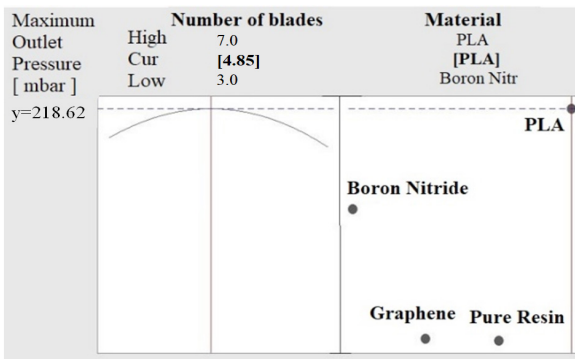
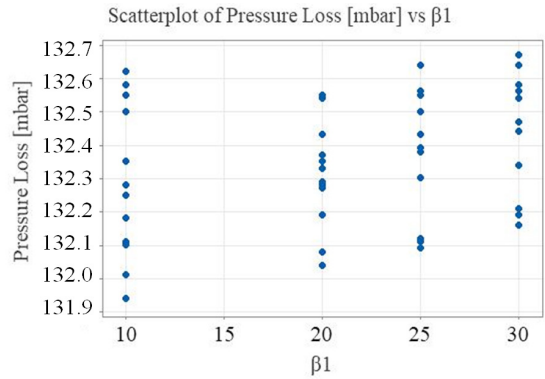
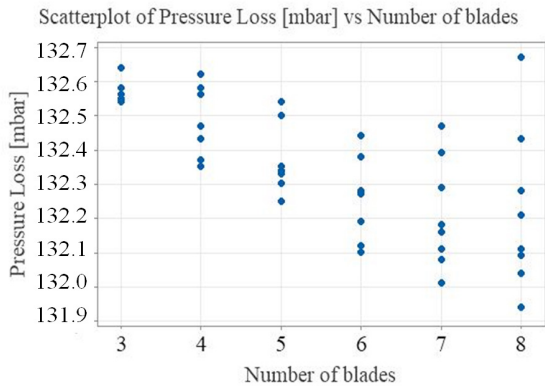


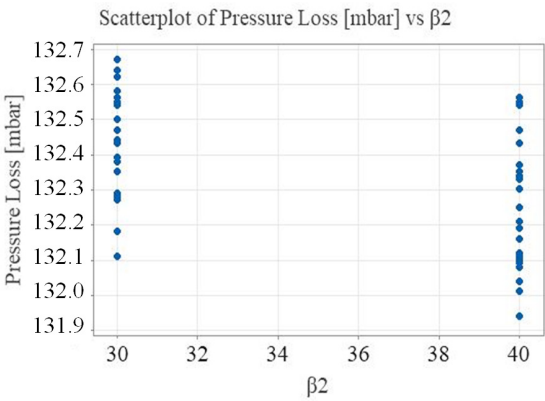
Fig. 16. Response optimization of outlet pressure for experimental measurements versus the number of blades and material



a)



b)



c)

Fig. 17. Pressure loss depending on: a) the number of blades, b) β_1 , and c) β_2

Fig. 17 shows the variation of the pressure loss and force acting on the blade depending on the number of blades, impeller inlet and outlet installation angles β_1 and β_2 , respectively.

Fig. 18 shows the effect of the determined parameters on the pressure loss and efficiency of impeller. Results from both experimental measurements and CFD analyses show the significant influence of the number of blades. These evaluations show that pressure losses will be significantly reduced if six-, seven-, or eight-bladed impellers are used. It is possible to say that the experimental results and the CFD analyses results are consistent with each other.

Although the results indicate the minimum pressure loss when the impeller blade pieces are increased, the values for the impeller with six, seven and eight blades, which give values close to this, were also examined. As the β_1 angle of the blade increases, the pressure loss increases, and as the β_2 angle increases, the pressure loss decreases. It has been seen that the pressure loss decreases as the number of blades increases. Considering all the results, the number of blades of the wheel should be six, seven, or eight. Considering the impeller efficiency, which is calculated inversely to the pressure loss, the efficiency of the impeller increases as β_1 decreases, β_2 increases, and the number of blades increases. The optimum values of the number of blades, inlet mounting angle β_1 and outlet mounting angle β_2 will be decided after statistical analysis in Minitab.

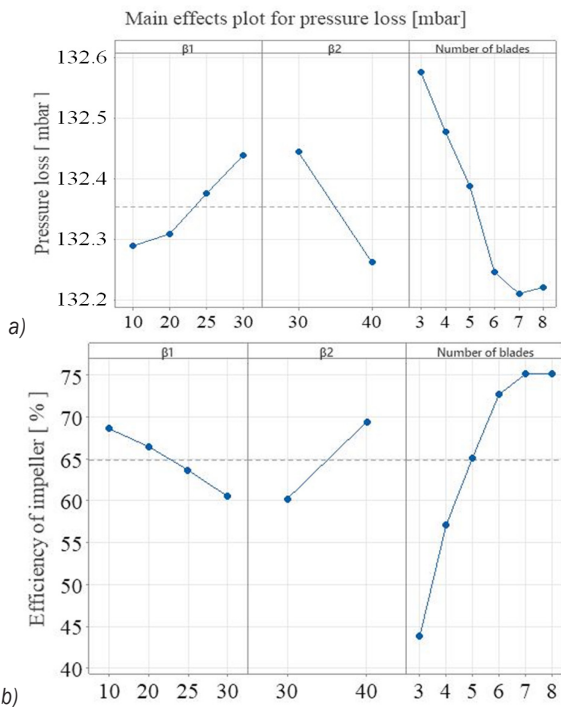


Fig. 18. Relationship between; a) pressure loss, and b) efficiency of impeller obtained by the CFD analyses and β_1, β_2 and number of blades

Fig. 19 shows the optimum values of the design parameters obtained after the regression analyses are performed. A new model was created using the parameters led by the regression analysis and CFD analyses were performed for this model. The response optimizer has been calculated according to the situation where the minimum pressure loss of the impeller efficiency is maximum. Fig. 20 shows the blade surface mesh image and total pressure

distribution graph for the suction and discharge sides. These values belong to optimum design as the response optimizer suggestion in the regression analysis. In this design, the pressure loss is calculated as 131.94 mbar and pump efficiency was calculated as 86.57 % at CFD analyses. According to the regression response optimizer tool, pressure loss will be 131.98 mbar, and impeller efficiency will be 89.47 %. The calculated values are so similar to each other. Also, a DOE factorial response optimizer has been applied; pressure loss has been seen at 131.89 mbar, and impeller efficiency has been seen at 91.09 %. The two different methods' results have been seen as similar to each other.

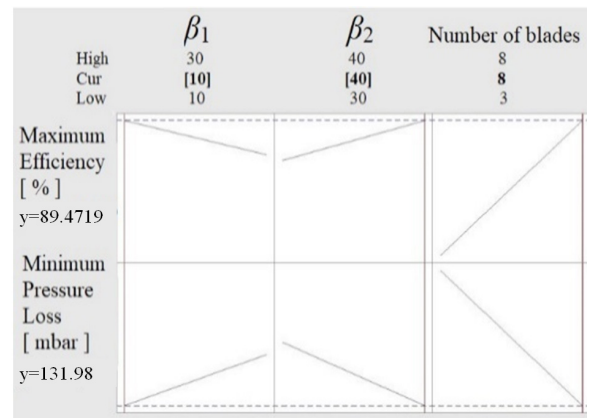


Fig. 19. Results of regression response optimization analysis using the findings by CFD analyses

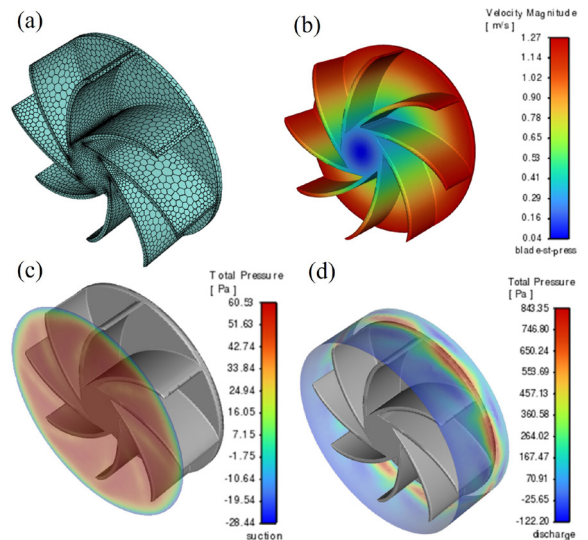


Fig. 20. Optimum design at $\beta_1=10^\circ, \beta_2=40^\circ$, number of blades = 8; a) blade surface mesh image, b) total velocity distribution, c) total pressure distribution at suction side, and d) total pressure distribution at discharge side

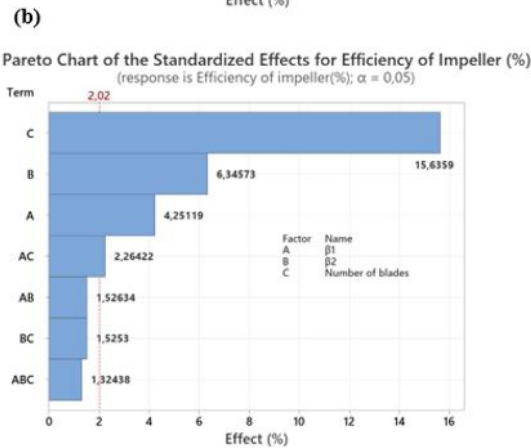
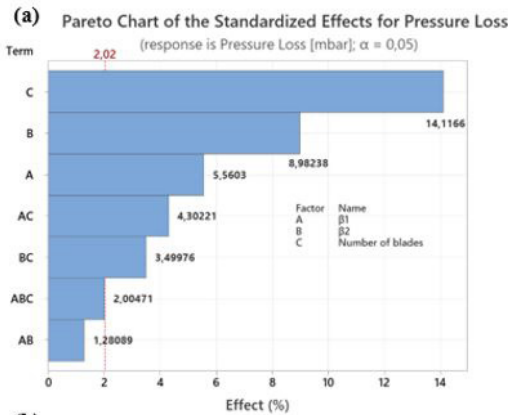
According to the response optimization of the results obtained in the experimental studies, as shown in Fig. 16, the optimum material should be PLA to keep maximum outlet pressure. Additionally, after all CFD analysis have been finished at 48 different designs, optimum design parameters obtained by the response optimizer analysis are determined as $\beta_1 = 10^\circ$, $\beta_2 = 40^\circ$, number of blades is 8. Fig. 19 shows these optimum design suggestions of response optimizer tool.

% in factorial regression analysis and the analysis is reliable since it is over 80 %.

Table 6 includes all results summary together. With the optimum design, approximately 6.5 % improvement in outlet pressure has been achieved compared to the design in conventional mass production. Impeller efficiency increased from 59.77 % to 86.57 %. With this optimization study, a design with minimum pressure loss and maximum impeller efficiency was obtained. As mentioned in the previous sections, while the pressure values by CFD analysis shows the pressures on the part, the outlet pressure in the experimental study shows the pressures taken from the lower spray arm nozzle after the impeller.

Table 6. Comparison of conventional and optimized impellers

	Efficiency of impeller [%]	Experimental outlet pressure [mbar]	Experimental pressure loss [mbar]	CFD analysis pressure loss [mbar]
Conventional design	59.77	220.5	130	132.5
Optimum design	86.57	234.8	116	131.94



c)

S	R-sq	R-sq(adj)	R-sq(pred)
4.96912	87.73 %	85.64 %	79.82 %

Fig. 21. Impact ratios of inputs for; a) pressure loss, b) efficiency of impeller, and c) factorial regression R-sq value

Fig. 21 shows the impact ratios of the design parameters on pressure loss and efficiency of impeller. The maximum effect among the parameters to reach the minimum pressure loss belongs to number of blades with 14.11 % and to reach maximum efficiency of impeller belongs to number of blades with 15.63 %. Also, the $R-sq(adj)$ value was also found to be 85.64

Within the scope of this study, a model was created with ANN using CFD analysis studies, and efficiency was predicted for the optimum parameters obtained from the response optimizer analyses.

Fig. 22 shows the training and prediction performances of the neural network used in this study. As can be seen, the tested values and the predicted values are quite close to each other, so it can be said that the ANN model is well trained. When all the results regarding the prediction performance of the neural network are considered, a match between the predicted and actual values is detected. As seen from the figure, the correlation factor for training is greater than 0.99. The developed ANN model has good interpolation capability and can be used as an efficient predictive tool for the outlet pressure of the valve. After ensuring that the neural network was trained for the entire database to achieve the best prediction accuracy, the impeller efficiency prediction for the optimal parameters was calculated using this model. For $\beta_1 = 10^\circ$, $\beta_2 = 40^\circ$, number of blades is 8, impeller efficiency was predicted as 82.6217 % using this ANN model. This result agrees with the results obtained from CFD analysis and response optimizer analysis.

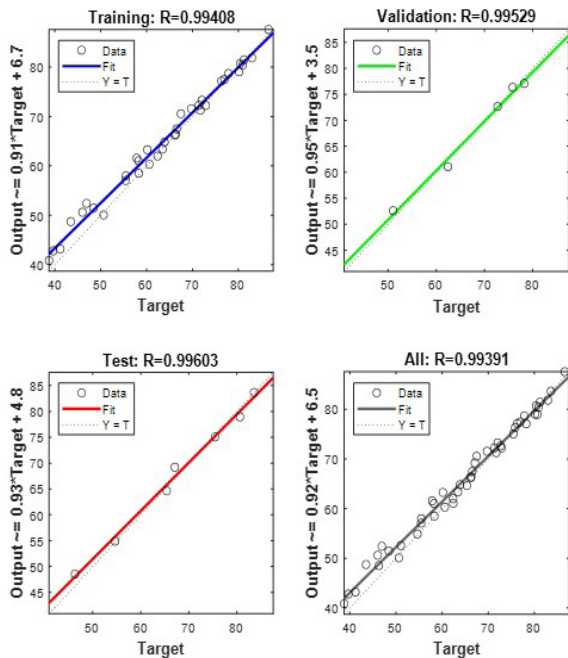


Fig. 22. Neural network training, validation, and test results regression results

4 CONCLUSIONS

This research investigates the effect of mechanical valve design on pressure loss in dishwasher systems. Within the scope of this study, a powerful methodology has been created for the design optimization of the impeller with the integration of experiments on real systems, CFD analysis, statistical analysis, and artificial neural network analysis. It has been concluded that the effectiveness of the impeller of the mechanical valve used in dishwashers depends on the blade profile's design and the number of blades. The results of this study also highlight the significance of material selection in the design and performance optimization of dishwasher mechanical valves. In this way, considering the findings obtained, it will contribute to the advancement of dishwasher technology by increasing the efficiency and effectiveness of the cleaning process, and saving energy. The research findings have practical implications for improving the performance of dishwashers and may contribute to the development of more efficient and reliable appliances in the future. The results of such research should be validated by practical tests in real-life dishwasher scenarios.

5 REFERENCES

- [1] Lu, B., Teng, J., Zhu, M., Qiang, X. (2023). Design optimization of a transonic compressor blade with sweep and lean integrated with axial slot casing treatment. *Aerospace Science and Technology*, vol. 136, art. ID 108225, DOI:10.1016/j.ast.2023.108225.
- [2] Rengma, T.S., Gupta, M.K., Subbarao, P.M.V. (2023). A novel method of optimizing the Savonius hydrokinetic turbine blades using Bezier curve. *Renewable Energy*, vol. 216, art. ID 119091, DOI:10.1016/j.renene.2023.119091.
- [3] Zhong, S., Jin, G., Ye, T. (2023). Isogeometric vibration and material optimization of rotating in-plane functionally graded thin-shell blades with variable thickness. *Thin-Walled Structures*, vol. 185, art. ID 110593, DOI:10.1016/j.tws.2023.110593.
- [4] Tang, D., Tang, B., Shen, W. Zhu, K., Quan, G. Deng, Z. (2023). On genetic algorithm and artificial neural network combined optimization for a Mars rotorcraft blade. *Acta Astronautica*, vol. 203, p. 78-87, DOI:10.1016/j.actaastro.2022.11.032.
- [5] Luo, J., Fu, Z., Fu, W., Chen, J. (2023). Aerodynamic optimization of a transonic fan rotor by blade sweeping using adaptive Gaussian process. *Aerospace Science and Technology*, vol. 137, art. ID 108255, DOI:10.1016/j.ast.2023.108255.
- [6] Lu, J., Zhang, F., Tao, R., Li, X., Zhu, D, Xiao, R. (2023). Optimization of runner and vane blade angle of an oscillating water column based on genetic algorithm and neural network. *Ocean Engineering*, vol. 284, art. ID115257, DOI:10.1016/j.oceaneng.2023.115257.
- [7] Fazil, J., Jayakumar, V. (2011). Investigation of airfoil profile design using reverse engineering Bezier curve. *Journal of Engineering and Applied Sciences*, vol. 6, no. 7, p. 43-52.
- [8] Fincham, J.H.S., Friswell, M.I. (2015). Aerodynamic optimisation of a camber morphing aerofoil. *Aerospace Science and Technology*, vol. 43, p. 245-255, DOI:10.1016/j.ast.2015.02.023.
- [9] Hansen, T.H. (2018). Airfoil optimization for wind turbine application. *Wind Energy*, vol. 21, no. 7, p. 502-514, DOI:10.1002/we.2174.
- [10] Jeong, J.H., Kim, S.H. (2018). Optimization of thick wind turbine airfoils using a genetic algorithm. *Journal of Mechanical Science and Technology*, vol. 32, no. 7, p. 3191-3199, DOI:10.1007/s12206-018-0622-x.
- [11] Salimi, A., Rostami, H.H., Riasi, A., Nejadali, J. (2023). Multi-objective optimization of a regenerative pump with S-shaped impeller using response surface methodology. *International Communications in Heat and Mass Transfer*, vol. 143, no. 106734, DOI:10.1016/j.icheatmasstransfer.2023.106734.
- [12] Satjaritanun, P., Regalbuto, J.R., Regalbuto, J.A., Tippayawong, N., Shimpalee, S. (2021). Mixing optimization with inward flow configuration contra-rotating impeller, baffle-free tank. *Alexandria Engineering Journal*, vol. 60, no. 4, p. 3759-3779, DOI:10.1016/j.aej.2021.02.045.
- [13] Mohammed, A.; Lemu, H. G., Sirahbizu, B. (2021). Determining optimum rotary blade design for wind-powered water-pumping systems for local selected sites. *Strojniški vestnik - Journal of Mechanical Engineering*, vol. 67, no. 5, p. 214-222, DOI:10.5545/sv-jme.2021.7104.

- [14] Zhang, H., Tang, L., Zhao, Y. (2020). Influence of blade profiles on plastic centrifugal pump performance. *Advances in Materials Science and Engineering*, vol. 2020, art. ID 6665520, DOI:10.1155/2020/6665520.
- [15] Elhosenya, M., Tharwat, A., Hassaniene, A.E. (2018). Bezier curve based path planning in a dynamic field using modified genetic algorithm. *Journal of Computational Science*, vol. 25, p. 339-350, DOI:10.1016/j.jocs.2017.08.004.
- [16] Wahba, W.A. (2001). *Design Optimization of Centrifugal Pump Impellers Using Parallel Genetic Algorithm*. PhD. Thesis, School of Mechanical Engineering, Department of Power, Propulsion and Aerospace Engineering, Cranfield University, Cranfield.
- [17] Matlab R2022a. (2022). from <https://www.mathworks.com/>, accessed on 2022-09-01.
- [18] Solidworks (2021). from <https://www.solidworks.com/>, accessed on 2022-07-07.
- [19] Bao, Y., Li T., Wang, D., Cai, Z., Gao, Z. (2020). Discrete element method study of effects of the impeller configuration and operating conditions on particle mixing in a cylindrical mixer. *Particology*, vol. 49, p. 146-158, DOI:10.1016/j.partic.2019.02.002.
- [20] Schmelzle, S., Leppert, S., Nirschl, H. (2015). Influence of impeller geometry in a vertical mixer described by DEM simulation and the dispersion model. *Advanced Powder Technology*, vol. 26, no. 5, p. 1473–1482, DOI:10.1016/j.appt.2015.08.003.
- [21] Eti Maden. (2023). Welfare Provided by Boron, from <https://www.etimaden.gov.tr/en/health>, accessed on 2023-06-02.
- [22] PCC Group. (2023). Graphene - what is it and what is it used for?, from <https://www.products.pcc.eu/en/blog/graphene-what-is-it-and-what-is-it-used-for>, accessed on 2023-07-05.
- [23] Acar Yavuz, G., Gören Kiral, B. (2022). Effect of cross-head speed on mechanical properties of photosensitive resins used in three-dimensional printing of a stereolithographic elastomer. *Materials Testing*, vol. 64, no. 11, p. 1675-1686. DOI:10.1515/mt-2022-0125.
- [24] Designer Data. POM (hom.) (2023). from [https://designerdata.nl/materials/plastics/thermo-plastics/polyoxymethylene-\(hom.\)](https://designerdata.nl/materials/plastics/thermo-plastics/polyoxymethylene-(hom.)), accessed on 2023-06-04.
- [25] Farah, S., Anderson, D.G., Langer, R. (2016). Physical and mechanical properties of PLA, and their functions in widespread applications - A comprehensive review. *Advanced Drug Delivery Reviews*, vol. 107, p. 367-392, DOI:10.1016/j.addr.2016.06.012.
- [26] Nanografi (2023). Graphene, from <https://nanografi.com/graphene/>, accessed on 2023-06-04.
- [27] Nanografi. Boron Nanoparticles (2023). from <https://nanografi.com/nanoparticles/element-alloys-nanoparticles/boron-nanoparticles/>, accessed on 2023-06-04.
- [28] Zhou, F., Sun, G., Zhang, Y., Ci, H., Wei, Q. (2018). Experimental and CFD study on the effects of surface roughness on cyclone performance. *Separation and Purification Technology*, vol. 193, p. 175-183, DOI:10.1016/j.seppur.2017.11.017.
- [29] ANSYS 2023R2. (2023). from <https://www.ansys.com>, accessed on 2023-07-24.
- [30] Minitab® 21.1. (2023). from <https://www.minitab.com>, accessed on 2023-07-23.
- [31] MathWorks. Deep Learning Toolbox, (2023). from <https://ww2.mathworks.cn/en/products/deep-learning.html>, accessed on 2023-05-05.
- [32] MathWorks. Improve neural network generalization and avoid overfitting (2023). from <https://ww2.mathworks.cn/help/deeplearning/deep-learning-with-simulink.html>, accessed on 2023-05-05.
- [33] Atilla, D., Sencan, C., Goren Kiral, B., Kiral, Z. (2020). Free vibration and buckling analyses of laminated composite plates with cutout. *Archive of Applied Mechanics*, vol. 90, p. 2433-2448, DOI:10.1007/s00419-020-01730-2.